Am J Transl Res 2018;10(5):1400-1412
www.ajtr.org /ISSN:1943-8141/AJTR0075362

Original Article

Comparative analysis of the two extremes of *FLNB*-mutated autosomal dominant disease spectrum: from clinical phenotypes to cellular and molecular findings

Qiming Xu[1], Nan Wu[1,3,4], Lijia Cui[5], Mao Lin[1], D Thirumal Kumar[6], C George Priya Doss[6], Zhihong Wu[2,3,4], Jianxiong Shen[1,3,4], Xiangjian Song[7], Guixing Qiu[1,3,4]

Departments of [1]Orthopedic Surgery, [2]Central Laboratory, Peking Union Medical College Hospital, Peking Union Medical College and Chinese Academy of Medical Sciences, Beijing, China; [3]Beijing Key Laboratory for Genetic Research of Skeletal Deformity, Beijing, China; [4]Medical Research Center of Orthopedics, Chinese Academy of Medical Sciences, Beijing, China; [5]Department of Endocrinology, Peking Union Medical College Hospital, Beijing, China; [6]Department of Integrative Biology, Vellore Institute of Technology, Vellore, India; [7]Department of Pediatric Orthopedics, Zhengzhou Orthopedic Hospital, Zhengzhou, Henan, China

Received March 3, 2018; Accepted April 18, 2018; Epub May 15, 2018; Published May 30, 2018

Abstract: Non-randomly distributed missense mutations of *Filamin B* (*FLNB*) can lead to a spectrum of autosomal dominant-inherited skeletal malformations caused by bone hypoplasia, including Larsen syndrome (LS), atelosteogenesi-I (AO-I), atelosteogenesi-I (AO-III) and boomerang dysplasia (BD). Among this spectrum of diseases, LS causes a milder hypoplasia of the skeletal system, compared to BD's much more severe symptoms. Previous studies revealed limited molecular mechanisms of *FLNB*-related diseases but most of them were carried out with HEK293 cells from the kidney which could not reproduce *FLNB*'s specificity to skeletal tissues. Instead, we elected to use ATDC5, a chondrogenic stem cell line widely used to study endochondral osteogenesis. In this study, we established *FLNB*-transfected ATDC5 cell model. We reported a pedigree of LS with mutation of $FLNB^{G1586R}$ and reviewed a case of BD with mutation of $FLNB^{L171R}$. Using the ATDC5 cell model above, we compared cellular and molecular phenotypes of BD-associated $FLNB^{L171R}$ and LS-associated $FLNB^{G1586R}$. We found that while both phenotypes had an increased expression of Runx2, $FLNB^{L171R}$-expressing ATDC5 cells presented globular aggregation of FLNB protein and increased cellular apoptosis rate while $FLNB^{G1586R}$-expressing ATDC5 cells presented evenly distributed FLNB protein and decreased cellular migration. These findings support our explanation for the cause of differences in clinical phenotypes between LS and BD. Our study makes a comparative analysis of two extremes of the *FLNB*-mutated autosomal dominant spectrum, relating known clinical phenotypes to our new cellular and molecular findings. These results indicated next steps for future research on the role of *FLNB* in the physiological process of endochondral osteogenesis.

Keywords: *FLNB*, larsen syndrome, boomerang dysplasia, ATDC5 cell, apoptosis

Introduction

Filamin B (FLNB) constitutes a large dimeric actin-binding protein to act as a cytoskeleton and multifunctional signal scaffold [1]. Nonrandomly-distributed missense mutations of *FLNB* can lead to a spectrum of autosomal-dominant inherited skeletal malformations caused by bone hypoplasia, including Larsen syndrome (LS, OMIM 150250), atelosteogenesis-I (AO-I, OMIM 108720), atelosteogenesis-III (AO-III, OMIM 108721) and boomerang dysplasia (BD, OMIM 112310). LS is at one extreme of the spectrum with the mildest hypoplasia of skeletal system, while BD is at the other extreme with the severest hypoplasia of skeletal system [2, 3]. LS presents skeletal deformities including scoliosis; cervical kyphosis; supernumerary carpal bones; dislocation of large joints; and characteristic facial malformations, including prominent forehead, wide-spaced eyes and depressed nasal bridge [4, 5]. BD is a lethal

skeletal dysplasia characterized by underdevelopment and potential lack of ossification in vertebrae, the acetabulum, or in the long bones of limbs, [6]. Almost all fetuses with BD die late in the prenatal stage, making it difficult to study the molecular mechanisms of *FLNB* in BD. AO-I and AO-III express traits between those associated with LS and BD. In addition to these diseases with *FLNB* missense mutations, nonsense mutations of *FLNB* can lead to spondylocarpotarsal synostosis syndrome (SCT, OMIM 272460), an autosomal recessive skeletal malformation characterized by premature fusion in carpal and tarsal joints and between the vertebrae leading to scoliosis and lordosis [10].

Mutations in *FLNB* are exclusively associated with skeletal diseases [4], indicating a high histological specificity of *FLNB* mutations' pathogenesis to the skeletal system. Multiple studies have attempted to explain the pathogenesis of *FLNB* mutations in skeletal malformation [3], including delay of ossification in growth plate of long bone [11], hypo-mobility of chondrocytes [12] and disturbance of proliferation; and differentiation and apoptosis in chondrocytes [13-15]. However, most of these studies were focused on nonsense mutations associated with SCT. Little literature has explained the pathogenic mechanisms of *FLNB* missense mutations in skeletal malformations due to complexity of this spectrum of diseases. Moreover, those studies were mostly carried out in HEK293 cells from the kidney, which may not be affected by *FLNB* in the same way as skeletal tissues.

In this study, we examine whether *FLNB* missense variants cause the difference between LS and BD at cellular and molecular levels. The target variants of LS were selected as c.4756G>A (p.Gly1586Arg) in *FLNB*, which was found in our LS patient, and another LS case reported by Krakow et al. [10], and the target mutation of BD was c.512T>G (p.Leu171Arg) in *FLNB*, which was reported in a male fetus diagnosed as BD [2, 6]. After transfecting *FLNB* plasmid to ATDC5 cell line, we compared distribution patterns of these two FLNB variants in cytoplasm, properties of cellular shape, cell migration, and apoptosis, and expression of Runx2 and Smad3 in endochondral osteogenesis. The cellular and molecular findings in our study sketched a logical chain to explain the difference in clinical phenotypes between LS and BD.

Material and methods

Clinical and radiological investigation

Our clinic recruited an eight-year old male with diagnosis of LS. We recorded the medical history of the patient and his family, then conducted physical and radiological examinations on body parts with potential skeletal malformation (**Figure 1**). The morbidity of BD was much rarer than LS. We chose a BD case with the mostly reported BD-associated mutation c.T512G (p.Leu171Arg) from literature [2, 6] as the research object for BD. Various phenotypes of those chosen objects of LS and BD were compared in details (**Table 1**).

Whole exome sequencing and Sanger sequencing

The study was approved by the Ethics Committee of Peking Union Medical College Hospital. With informed consent from the patient and his family members, we extracted DNA from peripheral blood samples of the patient, and his father, mother and sister using Puregene Blood kit. Whole exome sequencing was performed using the Illumina HiSeq 2000 (Illumina, San Diego, CA), reaching an average coverage of 116X. Reads were mapped to UCSC human genome reference assembly 19 (hg 19). Variant was called using BWA software (0.7.5a-r405). To identify pathogenic mutations, the variants were further compared to three databases including ClinVar, OMIM and HGMD; single nucleotide polymorphisms (SNP) among the normal population was excluded based five population-based databases, including 1000 Genomes Project Dataset, Exome Sequencing Project, Exome Aggregation Consortium dataset and Allele Frequency Net Database of Japan Tokyo and Netherlands. Mutations found in *FLNB* were further confirmed using Sanger sequencing. Exon 14 in *FLNB* was amplified using polymerase chain reaction (PCR), and sequenced in an Applied Biosystem 3730xl DNA Analyzer.

Plasmid construction and transfection

The wild-type *FLNB* plasmid was kindly donated by Stephen P. Robertson from Otago University,

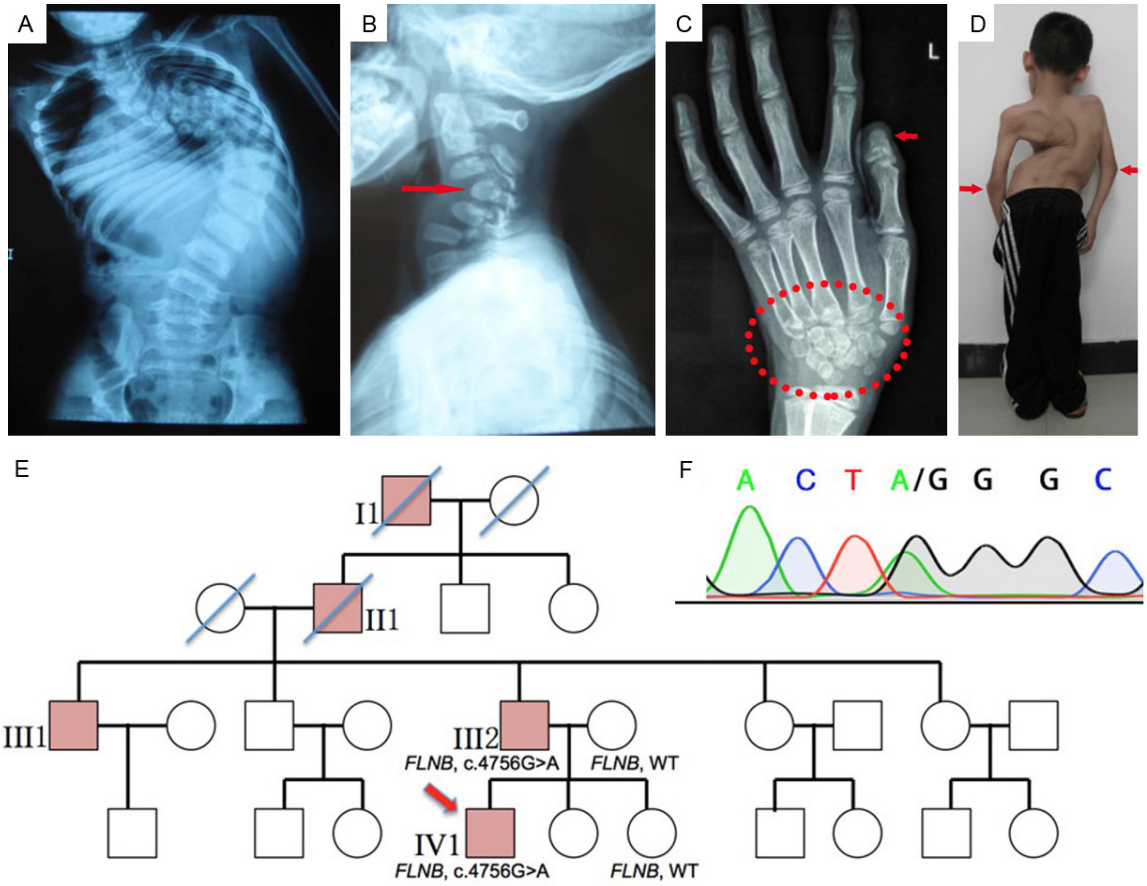

Figure 1. Clinical manifestation and family tree of the patient with Larsen syndrome. Whole spine X-ray and cervical spine X-ray revealed severe scoliosis (A) and cervical kyphosis with dysplasia of C4 and C5 vertebrae (B); hand and carpal joint X-ray showed supernumerary carpal bones and spatulate thumb; there should be eight carpal bones in a normal wrist while thirteen carpal bones were found in the wrist of this patient (C); gross anatomical pictures revealed serious back curves, short stature and varus deformities of elbow on both sides (D); The father (III2), uncle (III1), grandfather (II1) and great-grandfather (I1) had unusual faces, spatulate distal phalanges and varus deformities in both elbows similar to the patient (IV1) (E); A *FLNB* missense mutation (NM_001457.3, c.4756G>A (p.Gly1586Arg)) was identified in both the patient and his father, and was not found in the mother and sister (F).

Dunedin, New Zealand [2]. The full-length *FLNB* cDNA (reference sequence NM_001457.3), was assembled with EGFP on the C-terminal (from pCI-FLNB-EGFP [16]), and expressed in the vector pCR3.1(-) (Invitrogen, Carlsbad, CA). For LS associated mutation c.4756G>A (p.Gly1586Arg) and BD associated mutation c. 512T >G (p.Leu171Arg), PCR mutagenesis was performed with forward and reverse primers with single-nucleotide alteration. The sequence of the constructed mutation was confirmed by Sanger sequencing.

HEK293 cells were purchased from the cell bank of Peking Union Medical College and ATDC5 cells were kindly donated by Professor Qiping Zheng of the Medical College of Jiangsu University. Both HEK293 and ATDC5 cells were grown in DMEM containing 10% FCS under 37°C with 5% CO_2. Antibiotics-free media was changed before transfection. Plasmids of empty vector, wild-type *FLNB*, $FLNB^{G1586R}$, and $FLNB^{L171R}$ were transfected into ATDC5 cells respectively, using jet PRIME transfection reagent (Polyplus) according to the manufacturer's protocols. Those plasmids were transfected respectively into HEK293 cells using Lipofectamine2000 (Invitrogen). Cells were collected after transfection for 48 hours.

Immuno-detection and imaging

Transfected cells were fixed with 4% paraformaldehyde and stained with 0.5 μg/ml Hoechst.

Table 1. Comparative analysis of clinical phenotypes of LS and BD

Case	Proband gender	Mutation in FLNB NM_001457.3	Diagnosis	Hypo-dysplasia of mid-face	Hypo-dysplasia of vertebral	Absence of long bones	Supernumerary ossification centers	Spatulate fingers	Deformities beyond skeletal system
Case 1	Male	c.4756G>A (G1586R)	LS	+	+	-	+	+	-
Case 2 [10]	Male	c.4756G>A (G1586R)	LS	+	+	-	+	+	-
Case 3 [6]	Male	c.512T>G (L171R)	BD	+	+	+	-	-	-

Case 1 is the proband of an LS pedigree reported in this article, and the same mutation was also detected in Case 2 which was reported previously [10]. Case 3 was a previously reported BD case, which was a male fetus with premature delivery [6]. LS: Larsen Syndrome; BD: Boomerang Dysplasia; +, present; -, absent.

Phalloidin was used for mark the actin cytoskeleton. Cells were observed using Nikon Laser confocal microscope. Images were captured using with 20 ms exposure of UV path for Hoechst, 100 ms exposure of 488 nm Laser for EGFP and 1 s exposure of 590 nm path for phalloidin.

Apoptosis and migration

Cell suspension was made after transfection for 48 hours, and Hoechst was added to a concentration of 1 mg/ml in 37°C water bath for 7 min. Then the suspension was cooled down on ice and re-suspended with PBS. Propidium Iodide (PI) was added to the suspension with a concentration of 5 mg/ml. Cells were centrifuged, rinsed with PBS, and analyzed with flow cytometry. Hoechst staining was performed for early apoptosis of cells and Propidium Iodide (PI) staining was performed for late apoptosis of cells.

For the transwell migration assay, 40,000 cells were placed in the top chamber of each insert. The cells that migrated through the membrane and adhered to the lower surface of the membrane were fixed with 4% paraformaldehyde and stained with DAPI. For quantification, cells were counted under a microscope in four random fields.

Western blotting

The total protein was extracted after 48 hours of transfection. The protein concentration was determined with protein quantitative kit (BCA), and equivalent amounts of protein (12 ug). The total protein was separated on a 12% SDS-PAGE gel and transferred onto poly-vinylidene difluoride (PVDF) membranes (Millipore Corporation), which was incubated with primary antibodies overnight. Primary antibodies used were anti-Runx2 (1:1000; cat No. ab23981, Abcam), anti-pSmad3 (phospho T179) (1:500; cat No. ab193297, Abcam), anti-pSmad3 (phospho S423 + S425) (1:1000; cat No. ab52903, Abcam), anti-Smad3 (1:3000; cat No. ab75512, Abcam), and anti-GAPDH (1:1000; cat No. sc-25778, Santa Cruz). The membrane was then incubated with the anti-rabbit IgG (1:1000; cat No. 14708, CST) or anti-mouse IgG (1:1000; cat No. 14079, CST) after a final wash, and developed in enhanced chemiluminescence (ECL) reagent (Millipore).

Statistical analysis

Student's t test was performed for statistical analysis. Error bars indicate standard deviation (SD).

Results

Comparative analysis of clinical phenotypes between LS and BD

The LS patient recruited by our clinic was an 8-year old male (**Figure 1**). Physical examinations revealed characteristic faces (wide-spaced eyes and depressed nasal bridge), torticollis toward the left side, spatulate-shaped distal phalanges in the thumbs and hallux, and varus deformities in both elbows (**Figure 1D**). Investigation into his family history revealed that the father (III2), uncle (III1), grandfather (II1) and great-grandfather (I1) all had characteristic faces, spatulate distal phalanges and varus deformities in bilateral elbows similar to the patient (IV1) (**Figure 1E**). Hand and carpal joint X-rays of the patient showed supernumerary carpal bones and spatulate distal phalanges of thumbs on both sides (**Figure 1C**). Spine X-rays showed 60° cervical kyphosis from C2-C6 with hypoplasia of C4 and C5 vertebrae (**Figure 1B**), and severe scoliosis with 85° Cobb angle of upper thoracic curve and 125° Cobb angle of main thoracic curve (**Figure 1A**). We performed whole exome sequencing in this patient (IV1), together with his father (III2), mother and sister (**Figure 1E**). A missense mutation in *FLNB* (NM_001457.3, c.4756G>A (p.Gly1586Arg)) dominantly co-segregated with LS phenotype in this family and was further confirmed by Sanger sequencing (**Figure 1F**). With three web-based tools for mutation pathogenicity prediction, this mutation was predicted to be "tolerated" in SIFT (SIFT score 0.46), "disease causing" in Mutation Taster (*p*-value of 0.9999); and "probably damaging" in PolyPhen-2 (score of 1.000). The p.Gly1586Arg variant was a conservative amino acid substitution across species. Considering both clinical and genetic manifestations, we confirmed the diagnosis of Larsen syndrome to the patient. In addition to this case of LS, another LS case previous reported with the same mutation site [10] was also reviewed (**Table 1**).

The phenotypes of a BD case with the mutation of $FLNB^{L171R}$ were reviewed in **Table 1**

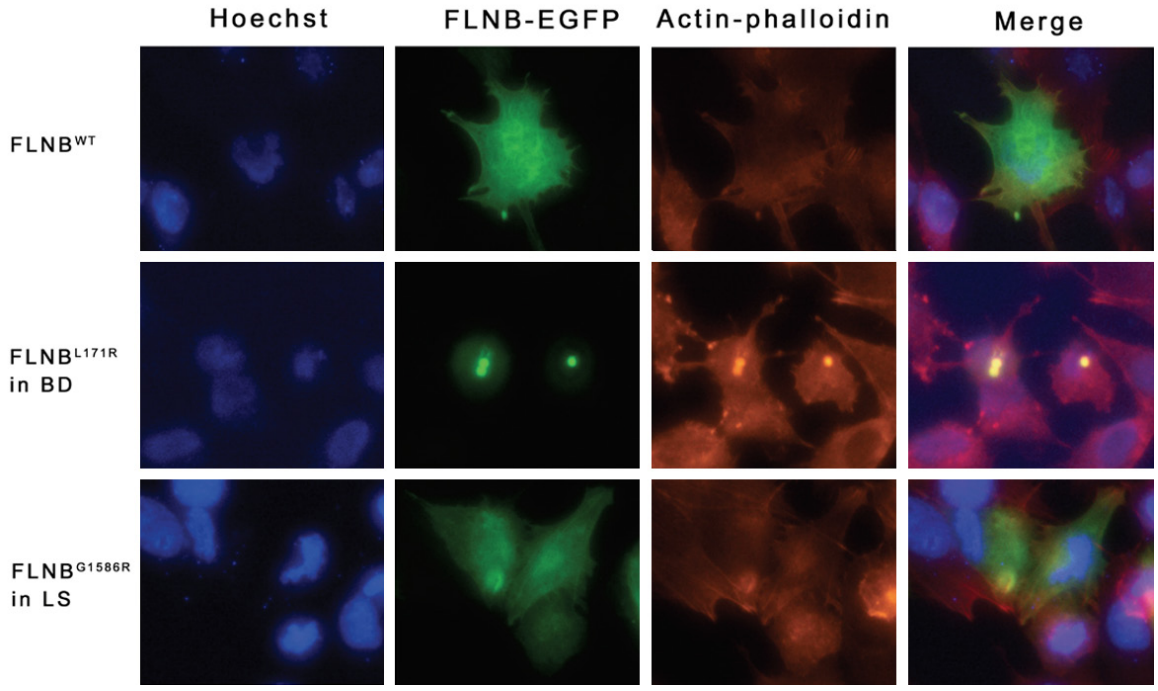

Figure 2. Accumulation of FLNB-actin in ATDC5 cells was visualized with confocal immunofluorescence microscopy. Nuclei were marked with Hoechst dye. In *FLNB^{WT}* transfected cells, the FLNB (EGFP marked) was evenly expressed in the cytoplasm consistently with the expression of actin cytoskeleton (phalloidin marked). In *FLNB^{L171R}* transfected ATDC5 (a mutation associated with BD), there were globular accumulations of FLNB and actin with the same localization of the cytoplasm. In *FLNB^{G1586R}* transfected ATDC5 (a mutation associated with LS), there was no obvious FLNB and actin accumulation. WT: wild type; BD: boomerang dysplasia; LS: Larsen syndrome.

according to a previous report [6]. The case involved a male fetus who presented thoracic hypoplasia and remarkable shortening of all extremities with disturbed ossifications, detected by ultrasonic scanning in his second trimester. Premature delivery occurred at 22 weeks' gestation. Post mortem examinations were consistent with the finding of previous ultrasonic scanning. Radiological imaging showed under-ossification and even absence of ossification centers of spine, pubis and long bones of extremities. The typical boomerang dysplasia was seen in long bones of both upper and lower extremities.

FLNB^{G1586R} and FLNB^{L171R} accumulated differently in ATDC5 cells, with changed cell shape, cell apoptosis and migration rates

Wild type *FLNB (FLNB^{WT})*, *FLNB^{G1586R}* and *FLNB^{L171R}* were transfected into HEK293 cells (Supplementary Figure 1) and ATDC5 cells (**Figure 2**), respectively. FLNB^{G1586R} expressed in HEK293 and ATDC5 cells was evenly distributed within the cytoplasm demonstrating a fine meshwork, and overlapped with the actin cytoskeleton. For *FLNB^{G1586R}* transfected cells, HEK293 cells demonstrated no obvious changes in cell shape, while ATDC5 cells transformed to a rounder and smaller cell configuration with less filopodias. However, in *FLNB^{L171R}* transfected HEK293 and ATDC5 cells, there showed a globular aggregation of FLNB, and ATDC5 cells also appeared an obvious shrank cell configuration and less filopodias.

FLNB^{L171R} transfected ATDC5 cells showed increased apoptosis ratio, as both the late apoptosis ratio and early apoptosis ratio were significantly higher than ATDC5 cells transfected with empty vector, *FLNB^{WT}* and *FLNB^{G1586R}* (**Figure 3**). However, there were no significant differences in apoptosis ratio among HEK293 cells transfected with empty vector, *FLNB^{WT}*, *FLNB^{L171R}* and *FLNB^{G1586R}* (Supplementary Figure 2).

Using Transwell Assay, *FLNB^{G1586R}* transfected ATDC5 cells showed significantly decreased migration rate, compared with ATDC5 cells

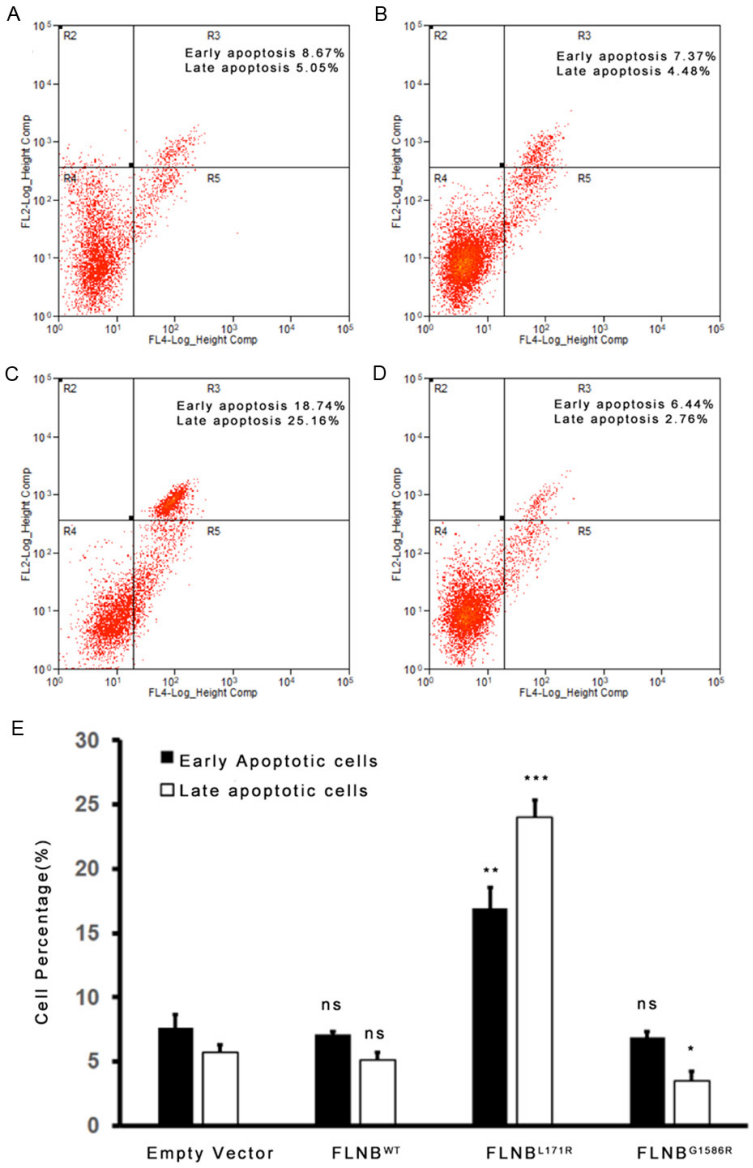

Figure 3. Apoptosis of ATDC5 cells was analyzed with flow cytometry. Hoechst staining was performed for early apoptosis of cells and Propidium Iodide (PI) staining was performed for late apoptosis of cells. ATDC5 cells expressing FLNB^{L171R} (a mutation associated with BD), presented a significantly higher apoptosis rate (C) than ATDC5 cells expressing empty vector (A), FLNB^{WT} (B) and FLNB^{G1586R} (a mutation associated with LS) (D). (E) Bar plot of percentages of apoptosis cells in different cell systems. Three experimental replicates were performed. Student's t-test was used for the statistical analysis. All values were compared to Empty vector group. ns: not significant; ***: *p*-value < 0.001; **: *p*-value < 0.01; *: *p*-value < 0.05. Error bars indicate SD. WT: wild type; BD: boomerang dysplasia; LS: Larsen syndrome.

transfected with empty vector, *FLNB^{WT}* and *FLNB^{L171R}* (**Figure 4**). Again, there was no difference in cell migration rate among HEK293 cells transfected with empty vector, *FLNB^{WT}*, *FLNB^{L171R}* and *FLNB^{G1586R}* (Supplementary Figure 3).

FLNB^{G1586R} and FLNB^{L171R} increased the expression of Runx2 and p-Smad3

Several molecular markers in osteogenesis were examined using Western blotting. Both the ATDC5 cells transfected with *FLNB^{L171R}* and those transfected with *FLNB^{G1586R}* had a significantly increased expression of Runx2 (**Figure 5**). Besides, the phosphorylated Smad3 (phosphorylation site: T179, and S423/S425) was increased in both ATDC5 cells expressing FLNB^{L171R} and those expressing FLNB^{G1586R}, while the expression of total Smad3 was not changed.

Discussion

A proper cell model is a prerequisite for carrying out rigorous cellular and molecular experiments. Though other researchers have reveals some important pathogenic mechanisms of *FLNB* missense mutations, those experiments were mostly carried out in HEK293 cells due to the relatively high transfection rate of plasmids [2, 17]. However, the HEK293 cell line from the kidney cannot mimic the skeletal developmental process. It is thus not a proper cell model for studies on FLNB, as FLNB is histologically specific to the skeletal system. On the other hand, ATDC5 is a chondrogenic stem cell line, which can be induced by insulin to display the whole differentiation stages of chondrocyte, including initial differentiation, condensation, proliferation, hypertrophy and mineralization [18]. We tried several transfection methods, and finally raised the transfection rate of *FLNB* plasmid in ATDC5 cells. Interestingly, ATDC5 cells did show some different properties from HEK293 cells. For example, changes in cell shapes, migration and

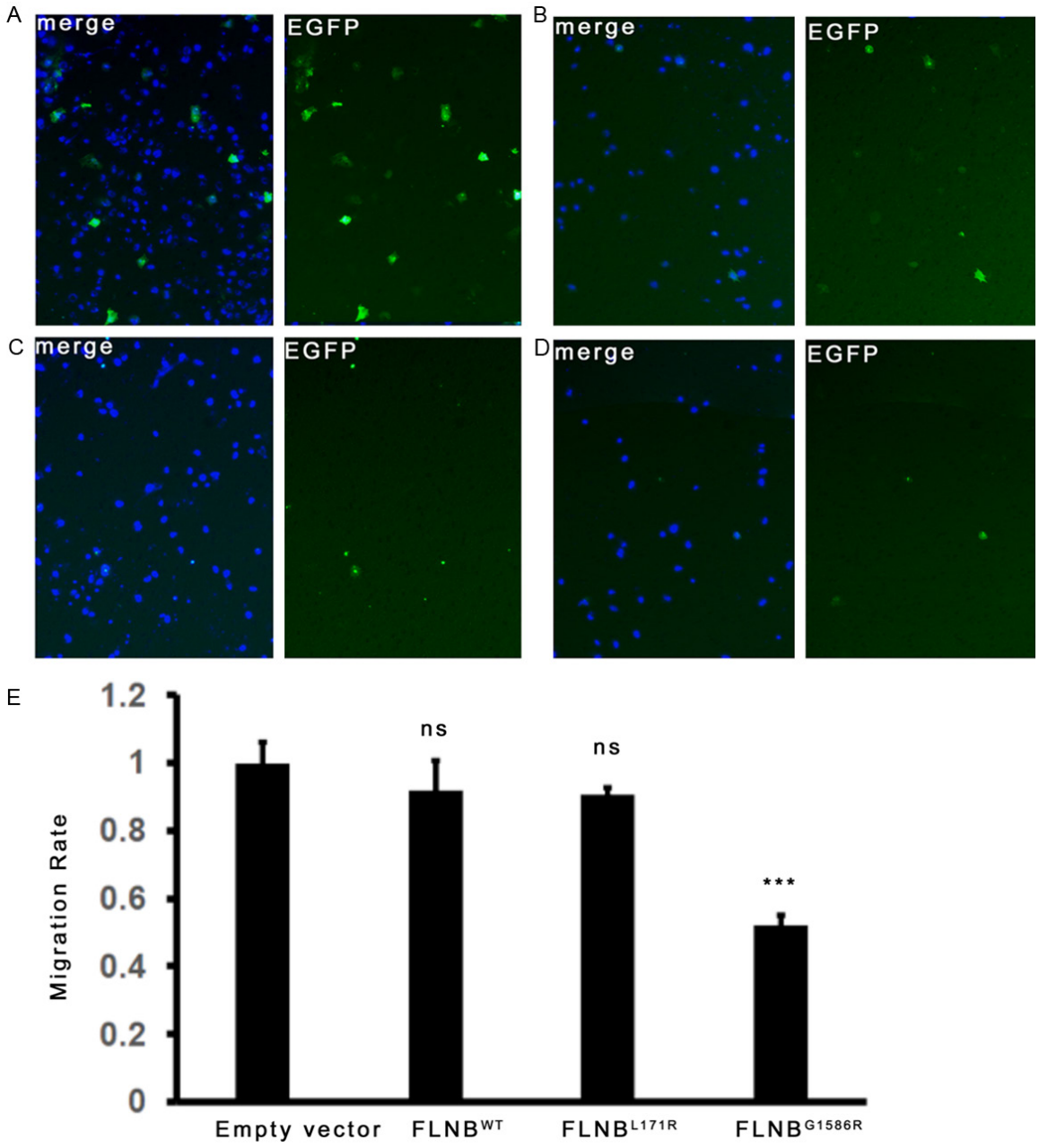

Figure 4. Transwell assay of ATDC5 cells expressing empty vector, $FLNB^{WT}$, $FLNB^{L171R}$ and $FLNB^{G1586R}$. The cells that migrated through the membrane and adhered to the lower surface of the membrane were fixed with 4% paraformaldehyde and stained with DAPI. For quantification, cells were counted under a microscope in four random fields. ATDC5 cells expressing $FLNB^{G1586R}$ (a mutation associated with LS) presented a significantly decreased migration rates (D), compared with ATDC5 cells expressing empty vector (A), $FLNB^{WT}$ (B), and $FLNB^{L171R}$ (a mutation associated with BD) (C). (E) Bar plot of cell migration rates in different cell systems. Three experimental replicates were performed. Student's t-test was used for the statistical analysis. All values were compared to Empty vector group. ns: not significant; ***: *p*-value < 0.001; **: *p*-value < 0.01; *: *p*-value < 0.05. Error bars indicate SD. WT: wild type; BD: boomerang dysplasia; LS: Larsen syndrome.

apoptosis were only observed in ATDC5 expressing $FLNB^{L171R}$ and $FLNB^{G1586R}$, but not in HEK293 cells expressing the same mutants. This result indicated that some biological and pathological functions of *FLNB* were cell type-dependent, which explained why *FLNB* muta-

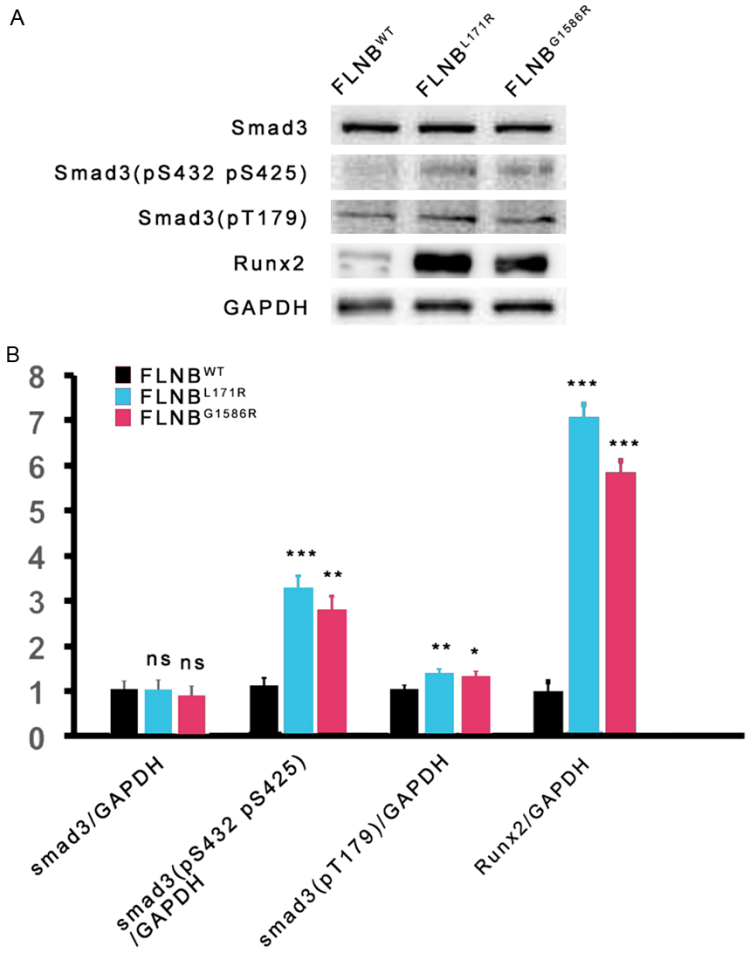

Figure 5. The expression of different molecular markers in osteogenesis in ATDC5 cells expressing empty vector, $FLNB^{WT}$, $FLNB^{L171R}$ (a mutation associated with BD) and $FLNB^{G1586R}$ (a mutation associated with LS), using Western blotting. The level of different proteins was compared relative to GAPDH. The expression of Runx2 was increased in both ATDC5 cells expressing $FLNB^{L171R}$ and $FLNB^{G1586R}$. The phosphorylated Smad3 (phosphorylation site: T179, and S423/S425) was increased in both ATDC5 cells expressing $FLNB^{L171R}$ and those expressing $FLNB^{G1586R}$, while the expression of total Smad3 was not changed compared with ATDC5 cells expressing $FLNB^{WT}$. Three experimental replicates were performed. Student's t-test was used for the statistical analysis. All values were compared to $FLNB^{WT}$ group. ns: not significant; ***: p-value < 0.001; **: p-value < 0.01; *: p-value < 0.05. Error bars indicate SD. WT, wild type; BD, boomerang dysplasia; LS, Larsen syndrome; GAPDH, glyceraldehyde-3-phosphate dehydrogenase.

tions solely caused diseases in the skeletal system.

Obvious transformation of cellular configuration was observed in ATDC5 cells expressing $FLNB^{L171R}$ and $FLNB^{G1586R}$, compared with ATDC5 cells expressing $FLNB^{WT}$. There was severe shrinkage of cell size and disappearance of lamellipodia in ATDC5 cells expressing $FLNB^{L171R}$, which could be attributed to the decreased actin cytoskeleton subsequent to the globular aggregation of $FLNB^{L171R}$ and actin. The amino acid position of 171 was located in the actin-binding domain (ABD) of FLNB. Enhanced actin-binding activity was firstly reported by Sawyer and colleagues' study on missense mutations in ABD of FLNB by in vitro and in vivo experiments [19]. The actin cytoskeleton mechanically supports the structure of cells, plays an important role in cell shaping and is essential for the survival of most cells [20]. ATDC5 cells expressing $FLNB^{G1586R}$ present less obvious alteration in their shapes, indicating the relatively intact actin cytoskeleton structure. The amino acid position of 1586 was close to the Hinge-1 domain of FLNB. Hinge-1 is a structure of flexibility which connects two parts of different important functions in Filamins (FLNs), and its deletion has been reported to change the mechanosensory properties of FLNs [21]. Instead of changes in the affinity between $FLNB^{G1586R}$ and actin, the cellular transformation of ATDC5 cells expressing $FLNB^{G1586R}$ was attributed to the changed property of nearby Hinge-1. Researchers found that the downstream domains beyond Hinge-1 in FLNA were involved in mechanical force changes and signal transduction [22, 23]. Thus, we propose that FLNB have a similar characteristic in Hinge-1, and its changed property may also affect downstream signaling pathways. The alteration of actin cytoskeleton (caused by $FLNB^{L171R}$) and downstream signaling changes (caused by $FLNB^{G1586R}$) would both change the cellular shaping process in endochondral osteogenesis, which may also alter the migration and apoptosis of cells; this will be discussed in the rest of this article.

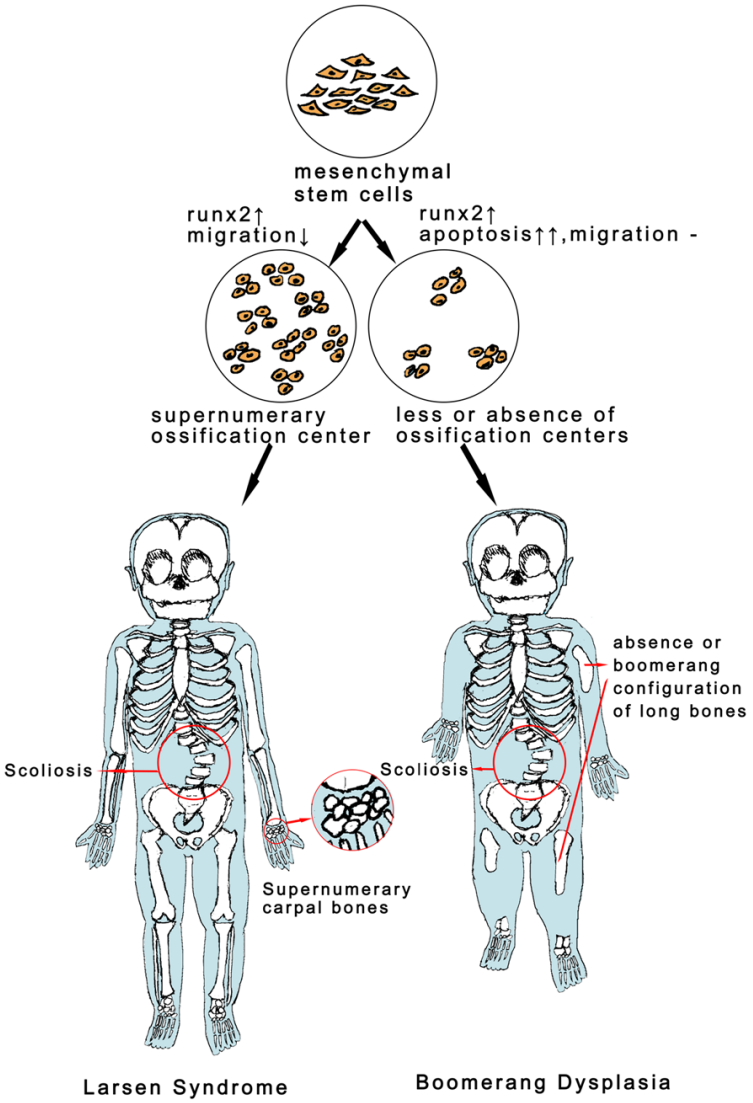

Figure 6. Schematic diagram on how different *FLNB* mutants lead to opposite phenotypes of BD and LS. Supernumerary ossification centers in LS and absence of ossification centers in BD may be resulted from counterbalance in mesenchymal cell apoptosis, mesenchymal cell migration and Runx2 expression. In LS, increased expression of Runx2 may promote the condensation of mesenchymal stem cells, while the decreased cellular migration, together with the promoted condensation, could lead to supernumerary ossification. In BD, though the expression of Runx2 was also increased, the much more increased cellular apoptosis rate might suppress Runx2's promotion in cellular condensation, and thus lead to decrease or absence of ossification centers. ↑, increase; ↓, decrease; ↑↑, increase with more extent; -, not changed; BD, boomerang dysplasia; LS, Larsen syndrome.

We propose that the difference in clinical phenotypes between LS and BD lies in the difference in apoptosis process (**Figure 6**). Actin cytoskeleton is essential to cell survival [20]. The apoptosis ratio of ATDC5 cells expressing FLNB^{L171R} abruptly increased, accompanying its diminished actin cytoskeleton, while in ATDC5 cells expressing FLNB^{G1586R}, the apoptosis ratio was unchanged, consistent with the little changed actin cytoskeleton. We suspect that it was the increased apoptosis that led to the absence of some long bones in FLNB^{L171R} caused BD patients. In the vertebrate, most of the skeleton including the long bones and the vertebral columns, are formed and developed through the endochondral osteogenesis [24], which originate from the condensation of mesenchymal cells to form ossification centers. Condensed mesenchymal cells can differentiate into chondrocytes [25]. Once the mineralization of extracellular matrix (ECM) and terminal hypertrophy occur, the chondrocytes undergo apoptosis and the cartilaginous structure converts into bony structure. Disturbance of chondrocyte apoptosis in any stages mentioned above can affect the procedure of endochondral osteogenesis. Previous studies have found an increased apoptosis of chondrocytes in *FLNB*$^{-/-}$ mice, however it was a model for SCT [14], which presented phenotypes opposite to BD. Non-induced ATDC5 cells have similar properties of mesenchymal cells before condensation [18]. Thus, the remarkably increased apoptosis in FLNB^{L171R} expressed ATDC5 cells inspired us that lethal skeletal hypoplasia and aplasia of long bones in BD [6] might be caused by disruption or absence of ossification center, which might be secondary to the increased apoptosis of mesenchymal cells during embryo development. In ATDC5 cells expressing FLNB^{G1586R}, we observed no changes of apoptosis ratio of cells. This finding is consistent with the clinical phenotypes of LS, as the hypoplasia in skeletal sys-

tem in LS is less severe than that in BD. This proposal and the underlying mechanism need to be verified in further studies.

The up-regulation of Runx2 in both ATDC5 cells expressing $FLNB^{L171R}$ and $FLNB^{G1586R}$ observed in our research was contradictory to the previous reports that Runx2 enhanced the endochondral osteogenesis [26]. Runx2, also called the core-binding factor (CBF), plays an essential role in osteogenesis [27, 28]. In the research of Zheng et al. [13], Smad3 was found to bind to FLNB protein to prevent Smad3 from being phosphorylated, while the free Smad3 can be phosphorylated. When phosphorylated Smad3 entered the nucleus, they interacted with both HDAC4 (histone deacetylase 4) and Runx2 to form a complex. In such situation, the activity of Runx2 can be repressed by HDAC4. In our study, although expression of Runx2 was increased in both $FLNB^{L171R}$ and $FLNB^{G1586R}$ expressed ATDC5 cells, the expression of phosphorylated Smad3 was also raised, indicating that the Runx2 activity was repressed and endochondral osteogenesis was also suppressed.

Runx2 also plays an important role in chondrogenesis (formation of cartilage), which is the prerequisite of endochondral osteogenesis. Akiyama et al. found that as ATDC5 cells condensed to cartilaginous nodules, and the expression of Runx2 increased through the whole process until the end of chondrocytic maturation [29]. The cellular condensation of undifferentiated ATDC5 cells and subsequent process were inhibited when dominant negative form of Runx2 was introduced to the cells. Decreased Runx2 inhibited the cellular condensation of ATDC5 cells through PI3K-Akt. And treatment of BMP-4 could rescue this inhibition by increasing the endogenous expression of Runx2. Thus, Runx2 may play a positive role in regulation of chondrogenesis. Those previous studies inspired us that the obvious increase of Runx2 in ATDC5 cells expressing $FLNB^{L171R}$ and $FLNB^{G1586R}$ may enhance the cellular condensation. From this point of view, the supernumerary carpal bones in the LS patients expressing $FLNB^{G1586R}$ may be caused by increased cellular condensation of mesenchymal cells during embryonic development (**Figure 6**). Also, the absence of long bones in BD patients expressing $FLNB^{L171R}$ could be explained by the deduction that the sharply increase apoptosis offset the enhanced condensation of mesenchymal cells.

Increased expression of Runx2 could also enhance the migration of ATDC5 cells through PI3K-Akt [30]. It was on contrary to the decreased migration of ATDC5 cells expressing $FLNB^{G1586R}$ observed in our study. We hypothesize that there is a balance between down-regulation of mutant FLNB and up-regulation of Runx2 in the migration of ATDC5 cells. Actin cytoskeleton plays an important role in cellular migration [31]. In ATDC5 cells expressing $FLNB^{G1586R}$, the actin cytoskeleton affected by $FLNB^{G1586R}$ could possibly diminish the cellular migration activity to an extent more than Runx2's up-regulation in cellular migration, because of a more direct effect of $FLNB^{G1586R}$ on actin cytoskeleton. Although $FLNB^{L171R}$ may also decrease the migration of ATDC5 cells, this process could be counterbalanced by the Runx2's up-regulation in cellular migration, because most $FLNB^{L171R}$ and F-actin, abnormally accumulated in cells, failed to function properly in cellular migration. Additionally, the paradox between accessory ossifications and hypoplasia of vertebrae column in LS [32] indicated a complicated counterbalance between decreased migration and cellular condensation of mesenchymal cells in the initial stage of osteogenesis of LS.

There are also limitations to this study. First, we only picked two mutation sites from BD and LS respectively to do in-vivo experiments. Further experiments should be applied to more mutation sites from autosomal dominant spectrum of *FLNB*-mutated diseases, to examine if the phenomena found in this study were universal. Second, cell models cannot represent the complete activities in the real developmental process. Thus, our group is now working on establishing an LS mouse model, to better understand the pathogenesis of *FLNB* missense mutations in skeletal malformations (unpublished data). Last, we transfected the mutated *FLNB* plasmids into ATDC5 cells, while the wildtype copy of endogenous *FLNB* gene was still active. However, this may not affect the comparison among groups, as the amount of endogenous wildtype FLNB was constant among different groups.

In this study, we brought forth the hypothesis that different missense mutated *FLNBs* lead to different phenotypes of skeletal malformations through the counterbalance of their effects on cell shape, apoptosis, migration and the downstream signaling. With ATDC5 cells transfected with $FLNB^{L171R}$ and $FLNB^{G1586R}$, we

simulated initial endochondral osteogenesis respectively in BD and LS, which are at two extremes of the spectrum of *FLNB* missense mutation-associated diseases. We sketched the scenario of how missense *FLNB* mutations took part in the skeletal malformations. For the next step, mutations associated with AO-I and AO-III, which present malformations overlapping BD and LS, will be verified with the same procedure in ATDC5 cells to complete the scenario. All these findings derived from the ATDC5 cell model should be further verified with animal models.

Acknowledgements

We acknowledge the family who participated in the research. We acknowledge Professor Stephen P. Robertson from Otago University, Dunedin, New Zealand for the donation of *FLNB* plasmids, and acknowledge Professor Qiping Zheng from Medical College of Jiangsu University for the donation of ATDC5 cells lines. This work was supported by National Natural Science Foundation of China (Nos. 81501852, 81472046 and 81472045), Beijing Natural Science Foundation (No. 7172175), Beijing nova program (No. Z161100004916123), Beijing nova program interdisciplinary collaborative project (No. xxjc201717), 2016 Milstein Medical Asian American Partnership Foundation Fellowship Award in Translational Medicine, Central Level Public Interest Program for Scientific Research Institute (No. 2016ZX310-177), PUMC Youth Fund & the Fundamental Research Funds for the Central Universities (No. 3332016006), CAMS Initiative for Innovative Medicine (No. 2016-I2M-3-003), Distinguished Youth foundation of Peking Union Medical College Hospital (No. JQ201506) and National Key Research and Development Program of China (No. 2016YFC0901501).

Disclosure of conflict of interest

None.

Address correspondence to: Dr. Xiangjian Song, Department of Pediatric Orthopedics, Zhengzhou Orthopedic Hospital, No. 58 Longhai Middle Road, Zhengzhou, Henan, China. Tel: +86-(0371)-67772-003; E-mail: sxj65@sina.com; Dr. Guixing Qiu, Department of Orthopedic Surgery, Peking Union Medical College Hospital, Peking Union Medical College and Chinese Academy of Medical Sciences, Beijing, China; Beijing Key Laboratory for Genetic Research of Bone and Joint Disease, Beijing, China; Medical Research Center of Orthopedics, Chinese Academy of Medical Sciences, No. 1 Shuaifuyuan, Beijing, China. Tel: +86-(010)-69152200; E-mail: qiuguixing-pumch@126.com

References

[1] Takafuta T, Saeki M, Fujimoto TT, Fujimura K and Shapiro SS. A new member of the LIM protein family binds to filamin B and localizes at stress fibers. J Biol Chem 2003; 278: 12175-12181.

[2] Daniel PB, Morgan T, Alanay Y, Bijlsma E, Cho TJ, Cole T, Collins F, David A, Devriendt K, Faivre L, Ikegawa S, Jacquemont S, Jesic M, Krakow D, Liebrecht D, Maitz S, Marlin S, Morin G, Nishikubo T, Nishimura G, Prescott T, Scarano G, Shafeghati Y, Skovby F, Tsutsumi S, Whiteford M, Zenker M and Robertson SP. Disease-associated mutations in the actin-binding domain of filamin B cause cytoplasmic focal accumulations correlating with disease severity. Hum Mutat 2012; 33: 665-673.

[3] Xu Q, Wu N, Cui L, Wu Z and Qiu G. Filamin B: the next hotspot in skeletal research? J Genet Genomics 2017; 44: 335-342.

[4] Robertson S. FLNB-related disorders. In: Pagon RA, Adam MP, Ardinger HH, Wallace SE, Amemiya A, Bean LJH, Bird TD, Fong CT, Mefford HC, Smith RJH, Stephens K, editors. GeneReviews (R). Seattle (WA): University of Washington; 1993.

[5] Larsen LJ, Schottstaedt ER and Bost FC. Multiple congenital dislocations associated with characteristic facial abnormality. J Pediatr 1950; 37: 574-581.

[6] Bicknell LS, Morgan T, Bonafe L, Wessels MW, Bialer MG, Willems PJ, Cohn DH, Krakow D and Robertson SP. Mutations in FLNB cause boomerang dysplasia. J Med Genet 2005; 42: e43.

[7] Greally MT, Jewett T, Smith WL Jr, Penick GD and Williamson RA. Lethal bone dysplasia in a fetus with manifestations of atelosteogenesis I and Boomerang dysplasia. Am J Med Genet 1993; 47: 1086-1091.

[8] Kozlowski K, Tsuruta T, Kameda Y, Kan A and Leslie G. New forms of neonatal death dwarfism. Report of 3 cases. Pediatr Radiol 1981; 10: 155-160.

[9] Urioste M, Rodriguez JI, Bofarull JM, Toran N, Ferrer C and Villa A. Giant-cell chondrodysplasia in a male infant with clinical and radiological findings resembling the Piepkorn type of lethal osteochondrodysplasia. Am J Med Genet 1997; 68: 342-346.

[10] Krakow D, Robertson SP, King LM, Morgan T, Sebald ET, Bertolotto C, Wachsmann-Hogiu S, Acuna D, Shapiro SS, Takafuta T, Aftimos S, Kim CA, Firth H, Steiner CE, Cormier-Daire V, Superti-Furga A, Bonafe L, Graham JM Jr, Grix

A, Bacino CA, Allanson J, Bialer MG, Lachman RS, Rimoin DL and Cohn DH. Mutations in the gene encoding filamin B disrupt vertebral segmentation, joint formation and skeletogenesis. Nat Genet 2004; 36: 405-410.
[11] Hu J, Lu J, Lian G, Ferland RJ, Dettenhofer M and Sheen VL. Formin 1 and filamin B physically interact to coordinate chondrocyte proliferation and differentiation in the growth plate. Hum Mol Genet 2014; 23: 4663-4673.
[12] Gardel ML, Schneider IC, Aratyn-Schaus Y and Waterman CM. Mechanical integration of actin and adhesion dynamics in cell migration. Annu Rev Cell Dev Biol 2010; 26: 315-333.
[13] Zheng L, Baek HJ, Karsenty G and Justice MJ. Filamin B represses chondrocyte hypertrophy in a Runx2/Smad3-dependent manner. J Cell Biol 2007; 178: 121-128.
[14] Lu J, Lian G, Lenkinski R, De Grand A, Vaid RR, Bryce T, Stasenko M, Boskey A, Walsh C and Sheen V. Filamin B mutations cause chondrocyte defects in skeletal development. Hum Mol Genet 2007; 16: 1661-1675.
[15] Hu J, Lu J, Lian G, Zhang J, Hecht JL and Sheen VL. Filamin B regulates chondrocyte proliferation and differentiation through Cdk1 signaling. PLoS One 2014; 9: e89352.
[16] van der Flier A, Kuikman I, Kramer D, Geerts D, Kreft M, Takafuta T, Shapiro SS and Sonnenberg A. Different splice variants of filamin-B affect myogenesis, subcellular distribution, and determine binding to integrin [beta] subunits. J Cell Biol 2002; 156: 361-376.
[17] Zhao Y, Shapiro SS and Eto M. F-actin clustering and cell dysmotility induced by the pathological W148R missense mutation of filamin B at the actin-binding domain. Am J Physiol Cell Physiol 2016; 310: C89-98.
[18] Shukunami C, Ishizeki K, Atsumi T, Ohta Y, Suzuki F and Hiraki Y. Cellular hypertrophy and calcification of embryonal carcinoma-derived chondrogenic cell line ATDC5 in vitro. J Bone Miner Res 1997; 12: 1174-1188.
[19] Sawyer GM, Clark AR, Robertson SP and Sutherland-Smith AJ. Disease-associated substitutions in the filamin B actin binding domain confer enhanced actin binding affinity in the absence of major structural disturbance: Insights from the crystal structures of filamin B actin binding domains. J Mol Biol 2009; 390: 1030-1047.
[20] Pollard TD and Cooper JA. Actin, a central player in cell shape and movement. Science 2009; 326: 1208-1212.
[21] Gardel ML, Nakamura F, Hartwig JH, Crocker JC, Stossel TP and Weitz DA. Prestressed F-actin networks cross-linked by hinged filamins replicate mechanical properties of cells. Proc Natl Acad Sci U S A 2006; 103: 1762-1767.
[22] Lad Y, Kiema T, Jiang P, Pentikainen OT, Coles CH, Campbell ID, Calderwood DA and Ylanne J. Structure of three tandem filamin domains reveals auto-inhibition of ligand binding. EMBO J 2007; 26: 3993-4004.
[23] Nakamura F, Heikkinen O, Pentikainen OT, Osborn TM, Kasza KE, Weitz DA, Kupiainen O, Permi P, Kilpelainen I, Ylanne J, Hartwig JH and Stossel TP. Molecular basis of filamin A-FilGAP interaction and its impairment in congenital disorders associated with filamin A mutations. PLoS One 2009; 4: e4928.
[24] Kronenberg HM. Developmental regulation of the growth plate. Nature 2003; 423: 332-336.
[25] Burdan F, Szumilo J, Korobowicz A, Farooquee R, Patel S, Patel A, Dave A, Szumilo M, Solecki M, Klepacz R and Dudka J. Morphology and physiology of the epiphyseal growth plate. Folia Histochem Cytobiol 2009; 47: 5-16.
[26] Yoshida CA and Komori T. Role of runx proteins in chondrogenesis. Crit Rev Eukaryot Gene Expr 2005; 15: 243-254.
[27] Merriman HL, van Wijnen AJ, Hiebert S, Bidwell JP, Fey E, Lian J, Stein J and Stein GS. The tissue-specific nuclear matrix protein, NMP-2, is a member of the AML/CBF/PEBP2/runt domain transcription factor family: interactions with the osteocalcin gene promoter. Biochemistry 1995; 34: 13125-13132.
[28] Sato M, Morii E, Komori T, Kawahata H, Sugimoto M, Terai K, Shimizu H, Yasui T, Ogihara H, Yasui N, Ochi T, Kitamura Y, Ito Y and Nomura S. Transcriptional regulation of osteopontin gene in vivo by PEBP2alphaA/CBFA1 and ETS1 in the skeletal tissues. Oncogene 1998; 17: 1517-1525.
[29] Akiyama H, Kanno T, Ito H, Terry A, Neil J, Ito Y and Nakamura T. Positive and negative regulation of chondrogenesis by splice variants of PEBP2alphaA/CBFalpha1 in clonal mouse EC cells, ATDC5. J Cell Physiol 1999; 181: 169-178.
[30] Fujita T, Azuma Y, Fukuyama R, Hattori Y, Yoshida C, Koida M, Ogita K and Komori T. Runx2 induces osteoblast and chondrocyte differentiation and enhances their migration by coupling with PI3K-Akt signaling. J Cell Biol 2004; 166: 85-95.
[31] Svitkina T. The actin cytoskeleton and actin-based motility. Cold Spring Harb Perspect Biol 2018; 10.
[32] Bicknell LS, Farrington-Rock C, Shafeghati Y, Rump P, Alanay Y, Alembik Y, Al-Madani N, Firth H, Karimi-Nejad MH, Kim CA, Leask K, Maisenbacher M, Moran E, Pappas JG, Prontera P, de Ravel T, Fryns JP, Sweeney E, Fryer A, Unger S, Wilson LC, Lachman RS, Rimoin DL, Cohn DH, Krakow D and Robertson SP. A molecular and clinical study of Larsen syndrome caused by mutations in FLNB. J Med Genet 2007; 44: 89-98.

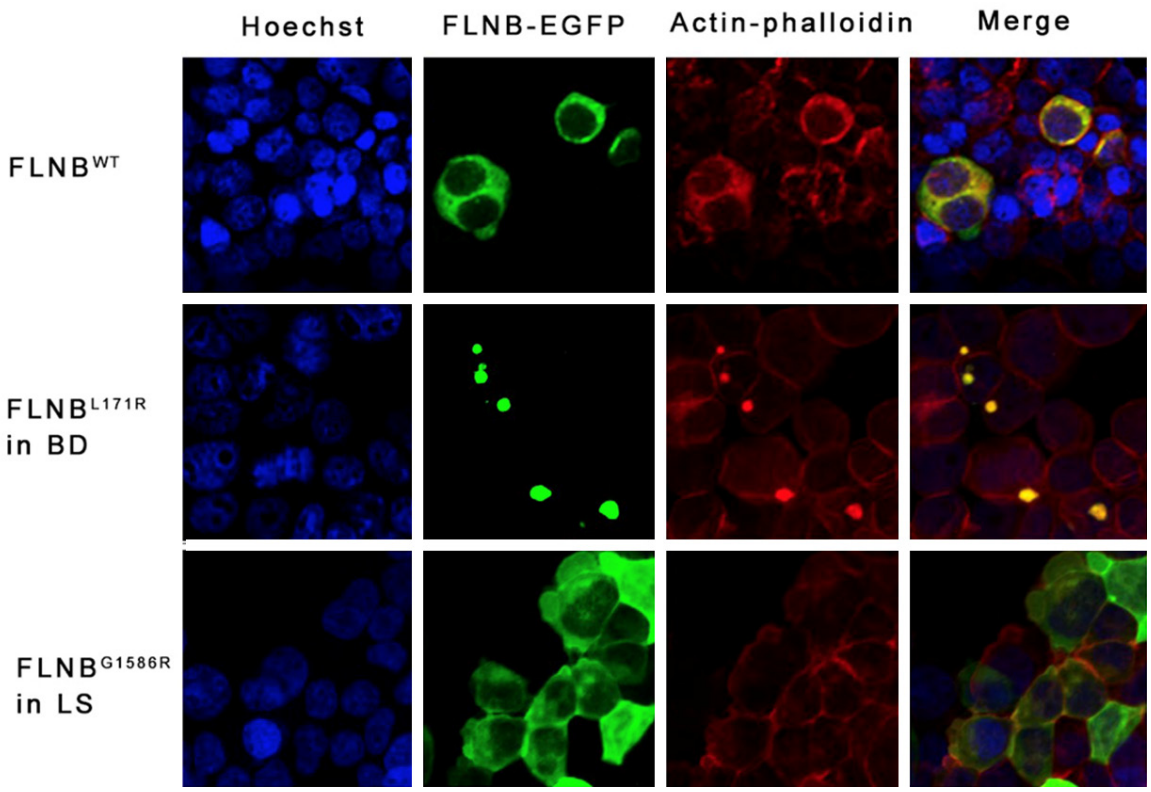

Supplementary Figure 1. *FLNB*, *FLNB*^{G1586R} and *FLNB*^{L171R} were transfected into HEK293 cells. Accumulation of FLNB-actin in HEK293 cells was visualized with confocal immunofluorescence microscopy. Nuclei were marked with Hoechst dye. In HEK293 cells expressing FLNB^{WT} and FLNB^{G1586R} (a mutation associated with LS), FLNB (EGFP marked) was evenly distributed within the cytoplasm demonstrating a fine meshwork, consistently with the expression of actin cytoskeleton (phalloidin marked). HEK293 cells expressing FLNB^{G1586R} demonstrated no obvious changes in cell shape. However, in HEK293 cells expressing FLNB^{L171R} (a mutation associated with BD), there showed a globular accumulation of FLNB. WT: wild type; BD: boomerang dysplasia; LS: Larsen syndrome.

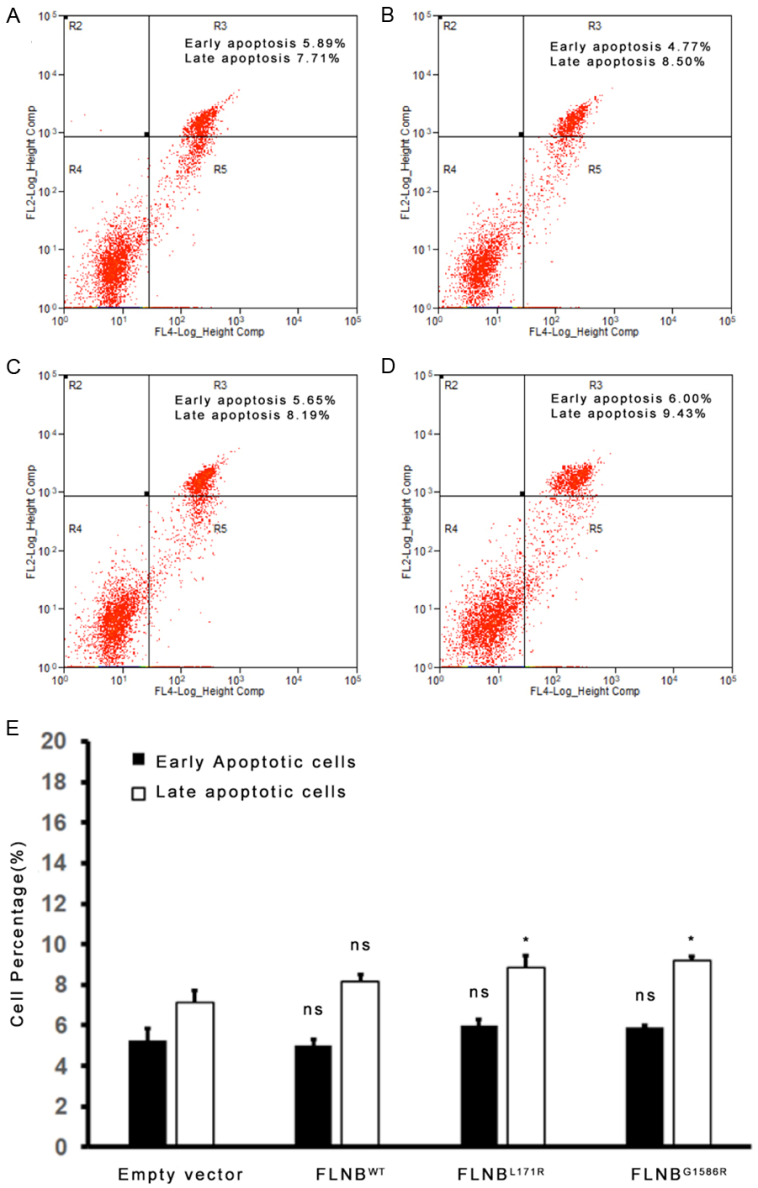

Supplementary Figure 2. Apoptosis of HEK293 cells was analyzed with flow cytometry. Hoechst staining was performed for early apoptosis of cells and Propidium Iodide (PI) staining was performed for late apoptosis of cells. There were no significant differences in apoptosis ratio among HEK293 cells expressing empty vector (A), $FLNB^{WT}$ (B), $FLNB^{L171R}$ (a mutation associated with BD) (C) and $FLNB^{G1586R}$ (a mutation associated with LS) (D). (E) Bar plot of percentages of apoptosis cells in different cell systems. Three experimental replicates were performed. Student's t-test was used for the statistical analysis. All values were compared to Empty vector group. ns: not significant; ***: *p*-value < 0.001; **: *p*-value < 0.01; *: *p*-value < 0.05. Error bars indicate SD. WT: wild type; BD: boomerang dysplasia; LS: Larsen syndrome.

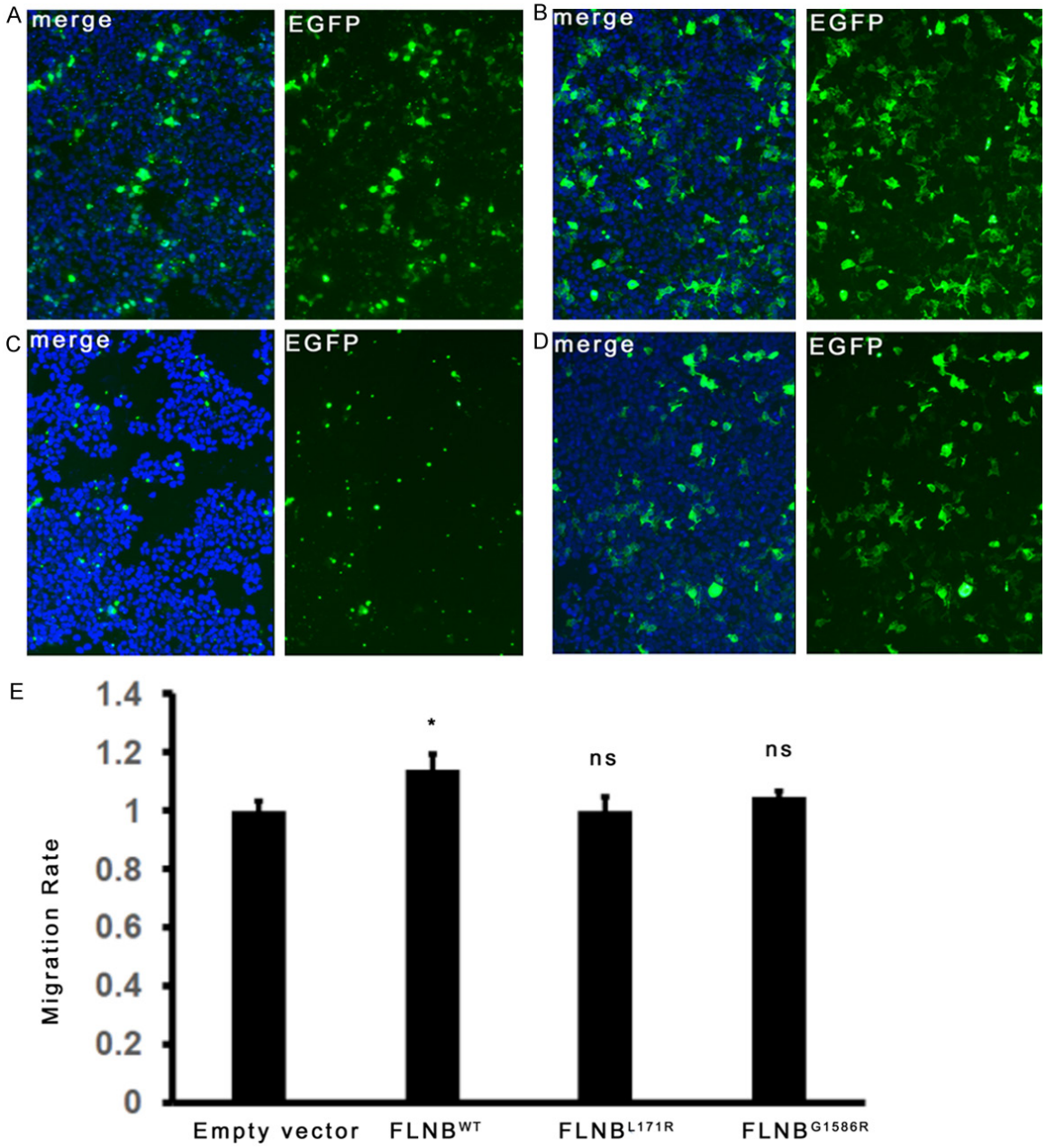

Supplementary Figure 3. Transwell assay of HEK293 cells expressing empty vector, FLNB^{WT}, FLNB^{L171R} and FLNB^{G1586R}. The cells that migrated through the membrane and adhered to the lower surface of the membrane were fixed with 4% paraformaldehyde and stained with DAPI. For quantification, cells were counted under a microscope in four random fields. There was no significant difference in cell migration rates among HEK293 cells expressing empty vector (A), FLNB^{WT} (B), FLNB^{L171R} (a mutation associated with BD) (C), and FLNB^{G1586R} (a mutation associated with LS) (D). (E) Bar plot of cell migration rates in different cell systems. Three experimental replicates were performed. Student's t-test was used for the statistical analysis. All values were compared to Empty vector group. ns: not significant; ***: *p*-value < 0.001; **: *p*-value < 0.01; *: *p*-value < 0.05. Error bars indicate SD. WT: wild type; BD: boomerang dysplasia; LS: Larsen syndrome.